AIAA JOURNAL
Vol. 41, No. 1, January 2003

Stable Numerical Method Applying a Total Variation Diminishing Scheme for Incompressible Flow

Byeong Rog Shin*
Tohoku University, Sendai 980-8577, Japan

To solve incompressible Navier–Stokes equations, a stable finite difference method applying a total variation diminishing (TVD) upwind scheme originally designed for compressible flow is proposed. The validity and the receptivity of this method employing such a TVD scheme for application to incompressible flow analysis are investigated by the evaluation of the accuracy, stability, and convergence rate. Using the generalized implicit simplified marker and cell (SMAC) solution method combined with the TVD scheme, three-dimensional developing entry flows through a square curved duct are calculated and compared with available experimental data and some computational results obtained by quadratic upstream interpolations for the convective kinematics (QUICK) schemes, as well as by third-order upwind schemes. The comparison shows that the TVD scheme has the highest computational efficiency without sharp loss of accuracy.

Nomenclature

g^{ij} = metric tensor, $\nabla\xi_i \cdot \nabla\xi_j$
H = entrance width of square duct
h_{ij} = metric tensor, $\partial x_k/\partial\xi_i \cdot \partial x_k/\partial\xi_j$
J = Jacobian, $\partial(x, y, z)/\partial(\xi, \eta, \zeta)$
p = static pressure
Re = Reynolds number, $U_0 H/\nu$
U_i = contravariant velocity components, $(\partial\xi_i/\partial x_j)u_j$
U_0 = inlet mean velocity
$\underline{\boldsymbol{u}}, u_i$ = physical velocity and its components
$\overline{u_i' u_j'}$ = Reynolds stress
$\boldsymbol{x}, x_i$ = Cartesian coordinate and its components
Z_i = contravariant vorticity components, $(\partial\xi_i/\partial x_j)\zeta_j$
Δt = time step
ϵ_{ijk} = permutation tensor in Eq. (3)
$\boldsymbol{\zeta}$ = $\nabla \times \boldsymbol{u}$
ζ_i = physical vorticity components
ν = kinematic viscosity
$\boldsymbol{\xi}, \xi_i$ = general curvilinear coordinate and its components
ϕ = pressure correction

Superscripts

m = mth approximation of Newton iteration
n = nth time level
$*$ = intermediate time level

I. Introduction

RECENTLY, because of its economical merits and high applicability, interest has been increasing in the computational fluid dynamics (CFD) approach as a design tool for advanced flow devices. Moreover, thanks to rapid advances in computer capability and the development of reliable CFD codes, it has become possible to some extent to analyze practical engineering flows accurately. However, many engineering flowfields, for instance, blade passages in turbomachinery or the flowfields around moving devices, have geometrically complex computational domains. Furthermore, flows may be unsteady, turbulent, and convection dominated. In practical computation, therefore, supercomputing with a large number of grid points and iterations is required, and the CFD code employed must be characterized by high efficiency, accuracy, and numerical stability.

In the computation of the convection-dominated flows such as high Reynolds number flows, the application of central difference approximations to the discretization of convection terms leads to numerical instability and nonphysical oscillations. To overcome these instabilities, therefore, the upwind method for the convection term in the Navier–Stokes equations is widely used, even though numerical diffusion is added to solutions. Because they guarantee the high accuracy of the solution despite the effect of numerical diffusion, higher-order upwind schemes such as the quadratic upstream interpolations for the convective kinematics (QUICK) family schemes[1,2] and the third-order upwind scheme are commonly used in calculations of incompressible flow. On the other hand, the total variation diminishing (TVD) schemes[3,4] are quite robust upwind schemes used for compressible flow problems. Actually, the application of such schemes for solving these flow problems has been very successful in the past decade. The primary reason for the increased popularity of high-speed flow simulation is that the TVD schemes utilize a limiting procedure to remove the local extremes, making this scheme capable of automatically generating nonoscillation and of obtaining favorable approximations to shocks and contact discontinuities. Generally, however, this scheme yields a solution that is of the first-order accuracy locally due to the operation of the limiting procedure.

The purpose of this paper is to propose a finite difference method combined with a TVD upwind scheme[4] for solving the incompressible Navier–Stokes equations and to investigate its receptivity. It is shown that even though the TVD scheme is designed for hyperbolic equations, its use is greatly advantageous in the simulation of practical incompressible flows, for which it is difficult to apply QUICK and modified QUICK (MQUICK) schemes as well as the third-order upwind scheme, because it reduces the numerical instability resulting from the calculation with common computational conditions without special treatments.

As a numerical example, a simulation of laminar, turbulent entry flow through a three-dimensional bent square duct[5,6] is performed because it is the most appropriate fluid dynamic device for understanding complex flow phenomena in curved passages encountered in a wide range of practical engineering applications. The numerical method used in this study is an efficient implicit simplified marker and cell (SMAC) scheme,[7,8] which has been developed by the author to solve the incompressible Navier–Stokes equations in curvilinear coordinates. Comparisons of predicted results from the TVD and other high-order upwind schemes with experimental data are provided to show the validity and feasibility of the present finite difference method combined with the TVD scheme used for the simulation of incompressible flows.

Presented as Paper 97-1868 at the AIAA 13th Computational Fluid Dynamics Conference, Snowmass Village, CO, 29 June–2 July 1997; received 4 April 2001; revision received 7 August 2002; accepted for publication 13 August 2002.

*Associate Professor, Institute of Fluid Science, Complex Flow Division; shin@ifs.tohoku.ac.jp. Senior Member AIAA.

II. Fundamental Equations and Numerical Method

A. Fundamental Equations of Curvilinear Coordinates

The fundamental equations are the continuity equation and the incompressible Navier–Stokes equations of volume fluxes JU_ℓ in curvilinear coordinates. They can be written as[7]

$$D \equiv \frac{\partial}{\partial \xi_i}(JU_i) = 0 \tag{1}$$

$$\frac{\partial}{\partial t}(JU_\ell) + L(JU_\ell, p) = 0, \qquad \ell = 1, 2, 3 \tag{2}$$

where

$$L(JU_\ell, p) \equiv \frac{\partial}{\partial \xi_i}(JU_iU_\ell) - JU_i\boldsymbol{u}\cdot\frac{\partial}{\partial \xi_i}\nabla\xi_\ell + \tilde{g}^{\ell i}\frac{\partial p}{\partial \xi_i} + \nu\epsilon_{\ell ij}\frac{\partial}{\partial \xi_i}\tilde{h}_{jk}JZ_k \tag{3}$$

where $\tilde{g}^{ij} = Jg^{ij}$ and $\tilde{h}_{ij} = h_{ij}/J$. In Eq. (2), the momentum equations of volume fluxes JU_ℓ correspond to the equations of flows through each cell side. Therefore, for the usual body-fitted curvilinear coordinate grid, the boundary condition can be imposed very easily. The second term on the right-hand side of Eq. (3) is an additional term introduced to express the convection term in conservative form, and the final term is the viscous diffusion term expressed in compact form using the contravariant vorticities.

In the turbulent flow computation, the large-eddy simulation (LES) method for the subgrid scale (SGS) turbulence is applied by adding the SGS stress term of $-J\nabla\xi_\ell(\nabla\cdot\overline{\boldsymbol{u}'\boldsymbol{u}'})$ to the right-hand side (RHS) of Eq. (3). In the present study, Smagorinsky's SGS turbulence model[9] employing the eddy viscosity ν_s is used as

$$-\overline{u_i'u_j'} = \nu_s\left(\frac{\partial u_i}{\partial x_j} + \frac{\partial u_j}{\partial x_i}\right) - \frac{2}{3}\delta_{ij}k_s \tag{4}$$

where

$$\nu_s = (C_s\Delta)^2\sqrt{2\bar{S}_{ij}\bar{S}_{ij}}, \qquad \bar{S}_{ij} = \frac{1}{2}\left(\frac{\partial u_i}{\partial x_j} + \frac{\partial u_j}{\partial x_i}\right) \tag{5}$$

Δ is the grid size, and C_s is the SGS coefficient. In the actual LES analysis, the turbulent energy k_s is not taken into account because it is so small.

Applying the fractional step method to Eq. (2), we have the following explicit SMAC scheme of curvilinear coordinates:

$$JU_\ell^* = JU_\ell^n - \Delta tL(JU_\ell, p)^n \tag{6}$$

$$JU_\ell^{n+1} = JU_\ell^* - \Delta t\tilde{g}^{\ell i}\frac{\partial\phi}{\partial \xi_i} \tag{7}$$

Then, taking the divergence of Eq. (7) and using Eq. (1) for JU_ℓ^{n+1}, we obtain the elliptic equation of pressure increment ϕ,

$$\frac{\partial}{\partial \xi_\ell}\left(\tilde{g}^{\ell i}\frac{\partial\phi}{\partial \xi_i}\right) = \frac{1}{\Delta t}\frac{\partial}{\partial \xi_\ell}\left(JU_\ell^*\right) \tag{8}$$

$$p^{n+1} = p^n + \phi \tag{9}$$

In this scheme, the dependent variables JU_ℓ and p are defined at different points of a staggered square grid in $\boldsymbol{\xi}$ space.[7] Using such a staggered grid is advantageous in that the occurrence of spurious errors are completely removed.

B. Implicit SMAC Scheme for Steady Flow

Now, Eq. (6) is extended to an implicit form by applying the delta-form approximate-factorization method[10] and partially including the viscous term in the left-hand side. Therefore, the momentum equations of the present implicit SMAC scheme are as follows[2]:

$$\left[1 + \Delta t\left(\frac{\partial}{\partial \xi}U^n - \nu\frac{\partial}{\partial \xi}\tilde{h}_{22}\tilde{h}_{33}\frac{\partial}{\partial \xi}\right)\right]\cdot\left[1 + \Delta t\left(\frac{\partial}{\partial \eta}V^n - \nu\frac{\partial}{\partial \eta}\tilde{h}_{33}\frac{\partial}{\partial \eta}\tilde{h}_{11}\right)\right]\cdot\left[1 + \Delta t\left(\frac{\partial}{\partial \zeta}W^n - \nu\frac{\partial}{\partial \zeta}\tilde{h}_{11}\frac{\partial}{\partial \zeta}\tilde{h}_{22}\right)\right]\Delta JU^* = \mathrm{RHS}_1^n \tag{10}$$

$$\left[1 + \Delta t\left(\frac{\partial}{\partial \xi}U^n - \nu\frac{\partial}{\partial \xi}\tilde{h}_{33}\frac{\partial}{\partial \xi}\tilde{h}_{22}\right)\right]\cdot\left[1 + \Delta t\left(\frac{\partial}{\partial \eta}V^n - \nu\frac{\partial}{\partial \eta}\tilde{h}_{33}\tilde{h}_{11}\frac{\partial}{\partial \eta}\right)\right]\cdot\left[1 + \Delta t\left(\frac{\partial}{\partial \zeta}W^n - \nu\frac{\partial}{\partial \zeta}\tilde{h}_{11}\frac{\partial}{\partial \zeta}\tilde{h}_{22}\right)\right]\Delta JV^* = \mathrm{RHS}_2^n \tag{11}$$

$$\left[1 + \Delta t\left(\frac{\partial}{\partial \xi}U^n - \nu\frac{\partial}{\partial \xi}\tilde{h}_{22}\frac{\partial}{\partial \xi}\tilde{h}_{33}\right)\right]\cdot\left[1 + \Delta t\left(\frac{\partial}{\partial \eta}V^n - \nu\frac{\partial}{\partial \eta}\tilde{h}_{11}\frac{\partial}{\partial \eta}\tilde{h}_{33}\right)\right]\cdot\left[1 + \Delta t\left(\frac{\partial}{\partial \zeta}W^n - \nu\frac{\partial}{\partial \zeta}\tilde{h}_{11}\tilde{h}_{22}\frac{\partial}{\partial \zeta}\right)\right]\Delta JW^* = \mathrm{RHS}_3^n \tag{12}$$

where

$$\mathrm{RHS}_\ell = -\Delta tL(JU_\ell, p), \qquad JU_\ell^* = JU_\ell^n + \Delta JU_\ell^* \tag{13}$$

This delta-formed implicit SMAC scheme satisfies a diagonally dominant condition with the first-order upwind difference scheme and is TVD stable. Also, this implicit SMAC scheme is suitable for vector or vector parallel machines[11] as compared with the highly SMAC scheme[12] and the semi-implicit method for pressure linked equations (SIMPLE) scheme[13] developed for scalar machines.

C. Implicit SMAC Scheme for Unsteady Flow

In the same manner as with Eqs. (10–12), Eq. (6) is extended to an unsteady implicit formulation. Therefore, the unsteady SMAC scheme is written as follows, for instance, with regard to JU in the ξ direction:

$$\left[1 + \Delta t\left(\frac{\partial}{\partial \xi}U^n - \nu\frac{\partial}{\partial \xi}\tilde{h}_{22}\tilde{h}_{33}\frac{\partial}{\partial \xi}\right)\right]\cdot\left[1 + \Delta t\left(\frac{\partial}{\partial \eta}V^n - \nu\frac{\partial}{\partial \eta}\tilde{h}_{33}\frac{\partial}{\partial \eta}\tilde{h}_{11}\right)\right]\cdot\left[1 + \Delta t\left(\frac{\partial}{\partial \zeta}W^n - \nu\frac{\partial}{\partial \zeta}\tilde{h}_{22}\frac{\partial}{\partial \zeta}\tilde{h}_{11}\right)\right]\times\Delta JU^{*(m)} = \mathrm{RHS}_1^{(m-1)} \tag{14}$$

where

$$\mathrm{RHS}_1^{(0)} = -\Delta tL(JU, p)^n, \qquad \mathrm{RHS}_1^{(m)} = \mathrm{RHS}_1^{(m-1)} + \Delta\mathrm{RHS}_1^{(m)}$$

$$\Delta\mathrm{RHS}_1^{(m)} = -\left[JU^{(m)} - JU^{(m-1)}\right] - \frac{1}{2}\Delta t\left(F_1^{(m)} - F_1^{(m-1)}\right) \quad \text{for} \quad m \geq 1 \tag{15}$$

$$F_1 = \frac{\partial}{\partial \xi_i}(JU_iU) + \tilde{g}^{\ell i}\frac{\partial p}{\partial \xi_i} + \nu\epsilon_{\ell ij}\frac{\partial}{\partial \xi_i}(\tilde{h}_{jk}JZ_k)$$

$$JU^{*(m)} = JU^{(m-1)} + \Delta JU^{*(m)}$$

$$JZ_\ell = \epsilon_{\ell ij}\frac{\partial}{\partial \xi_i}(\tilde{h}_{jk}JU_k), \qquad \ell = 1, 2, 3$$

When the solution converges, Eq. (14) is always reduced to the Crank–Nicholson method. In the same way, Eqs. (7–9) can be written as follows:

$$JU_\ell^{(m)} = JU_\ell^{*(m)} - \frac{1}{2}\Delta t\tilde{g}^{\ell i}\frac{\partial\phi^{(m)}}{\partial \xi_i} \tag{16}$$

$$\frac{\partial}{\partial \xi_\ell}\left(\tilde{g}^{\ell i}\frac{\partial\phi^{(m)}}{\partial \xi_i}\right) = \frac{1}{\Delta t}\frac{\partial}{\partial \xi_\ell}\left(JU_\ell^{*(m)}\right) \tag{17}$$

$$p^{(m)} = p^{(m-1)} + \phi^{(m)} \tag{18}$$

In Eqs. (14–18), the superscript m denotes the number of Newton iterations.

In this implicit SMAC scheme for unsteady flow, the solutions at each time step JU_ℓ^{n+1} and p^{n+1} are obtained from Eqs. (14–18) of

the Newton iteration. The RHSs of Eqs. (14) and (17) represent the residuals of Eqs. (2) and (1), respectively, and $\Delta JU^{*(m)}$ and $\phi^{(m)}$ of the left-hand sides are the corrections of JU and p at each iteration. If the values of these residuals are close to zero, then the corrections also tend to zero, and the solution converges. The accuracy of the solution depends only on the RHSs and is independent of the left-hand sides.

Equations (10–12) and Eq. (14) can be solved by dividing them into three steps; each step is a problem that is solved by the simultaneous linear equations with tridiagonal matrix by Gaussian elimination. The simultaneous linear equations (8) and (17) are solved by the vectorized Tschebyscheff successive line overrelaxation method in which sweep directions are alternated as in the alternating direction implicit method, which is suitable in supercomputing. In this study, Eqs. (14–17) were discretized in the same way as in Ref. 8.

III. Upwind Difference Schemes

The second-order central difference is basically used for the space derivatives. However, for the convection term on the left-hand side of Eqs. (10–12) and Eq. (14), the first-order upwind difference scheme is used to reduce computational effort and to accelerate the convergency, whereas the higher-order upwind difference scheme is applied to the RHS to solve the high-Reynolds-number flow with accuracy and stability. Here, a simple one-dimensional equation is considered to explain the upwind schemes as

$$\frac{\partial u}{\partial t}+\frac{\partial f(a,u)}{\partial x}=\frac{\partial u}{\partial t}+a\frac{\partial u}{\partial x}=0 \tag{19}$$

where $a(u)=\partial f/\partial u$ is the propagating speed of waves or the transport speed of the convection term. The finite difference equation of Eq. (19) can generally be written in the conservation form

$$u_i^{n+1}+\lambda\theta\left(\hat{f}_{i+\frac{1}{2}}-\hat{f}_{i-\frac{1}{2}}\right)^{n+1}=u_i^n-\lambda(1-\theta)\left(\hat{f}_{i+\frac{1}{2}}-\hat{f}_{i-\frac{1}{2}}\right)^n \tag{20}$$

where $\lambda=\Delta t/\Delta x$, $0\le\theta\le 1$, and $\hat{f}$ is the numerical flux function. In the case of the second-order central difference scheme, the numerical flux function is taken as $\hat{f}_{i+1/2}=a_{i+1/2}(u_i+u_{i+1})/2$.

A. MQUICK and the Third-Order Upwind Scheme

As a general form of the upwind finite difference scheme with fourth-order artificial dissipation, the numerical flux in Eq. (20) is written as

$$\hat{f}_{i+\frac{1}{2}}=a_{i+\frac{1}{2}}\{-(1+\alpha)u_{i-1}+(c_1+3\alpha)u_i+(c_1-3\alpha)u_{i+1}-(1-\alpha)u_{i+2}\}/c_2 \tag{21}$$

with $\alpha=\alpha_0\,\mathrm{sign}(a_{i+1/2})$. In the QUICK scheme,[1] the values $\alpha_0=1$, $c_1=9$, and $c_2=16$ in Eq. (21) are chosen. Also, in the MQUICK scheme,[2] which has better numerical stability and a higher convergence rate than the original QUICK scheme, $\alpha_0=4$ is generally adopted. On the other hand, for the third-order upwind scheme, $\alpha_0=1$, $c_1=7$, and $c_2=12$ are employed.

B. TVD Upwind Scheme

The higher-order TVD scheme is expressed as a sum of the first-order upwind scheme and correction terms that function to realize higher-order schemes, and then the correction terms are modified locally by a limiter to stabilize the solution. The numerical flux of the Chakravarthy–Osher TVD upwind scheme[4] becomes

$$\begin{aligned}\hat{f}_{i+\frac{1}{2}}&=(f_i+f_{i+1})/2\\&\quad-\left(Df^+_{i+\frac{1}{2}}-Df^-_{i+\frac{1}{2}}\right)\Big/2\Big] && \text{Roe's first upwind}\\&\quad+\frac{1-\kappa}{4}d\tilde{f}^+_{i-\frac{1}{2}}+\frac{1+\kappa}{4}d\tilde{f}^+_{i+\frac{1}{2}} && \left(a_{i+\frac{1}{2}}\ge 0\right)\\&\quad-\underbrace{\frac{1-\kappa}{4}d\tilde{f}^-_{i+\frac{3}{2}}}_{\text{2nd upwind}}-\underbrace{\frac{1+\kappa}{4}d\tilde{f}^-_{i+\frac{1}{2}}}_{\text{2nd central}} && \left(a_{i+\frac{1}{2}}<0\right)\end{aligned} \tag{22}$$

Here, the flux-limited values of df and the minmod function are determined by

$$d\tilde{f}^{\pm}_{i+\frac{1}{2}}=\mathrm{minmod}\left(Df^{\pm}_{i+\frac{1}{2}},bDf^{\pm}_{i+\frac{3}{2}}\right)$$

$$d\tilde{f}^{\pm}_{i+\frac{1}{2}}=\mathrm{minmod}\left(Df^{\pm}_{i+\frac{1}{2}},bDf^{\pm}_{i-\frac{1}{2}}\right)$$

$$\mathrm{minmod}(x,y)=\mathrm{sign}(x)\max[0,\min\{|x|,y\,\mathrm{sign}(x)\}] \tag{23}$$

and $Df^{\pm}_{i+1/2}=a^{\pm}_{i+1/2}\Delta u_{i+1/2}$, $a^{\pm}=(a\pm|a|)/2$, and $\Delta u_{i+1/2}=u_{i+1}-u_i$. The parameter κ is a linear combination parameter determined by the range of $-1\le\kappa\le 1$ and affects the accuracy of Eq. (22). According to the Taylor expansion, the truncation error for the unlimited forms of the TVD scheme in Eq. (22) is expressed as $-\frac{1}{12}(3\kappa-1)\Delta x^2 f_{xxx}+\mathcal{O}(\Delta x^3)$. Therefore, we know that the TVD scheme of Eq. (22) has a third-order accuracy at $\kappa=\frac{1}{3}$ and that at the other values of κ it becomes a second-order scheme. Particularly for the κ of -1, 0, $\frac{1}{2}$, and 1, Eq. (22) becomes a second-order

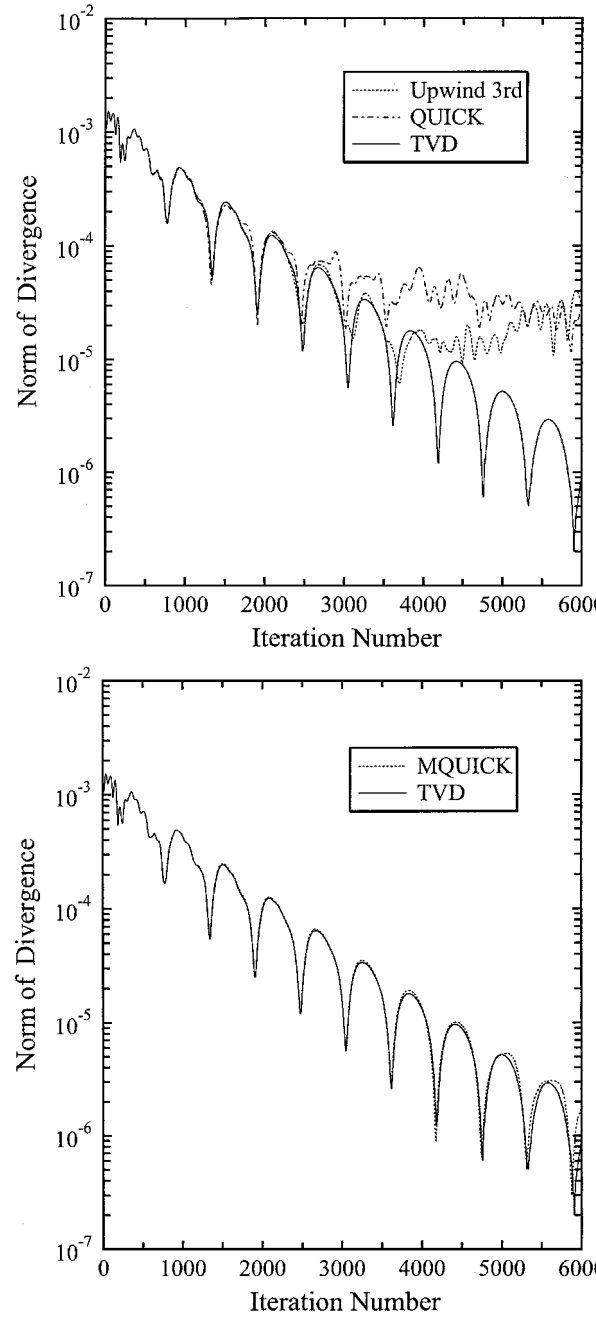

Fig. 1 Comparison of iteration history of norm of divergence.

upwind scheme, Fromm's scheme (see Ref. 14), QUICK scheme, and central difference scheme, respectively. On the other hand, the slope of the flux in the minmod function of Eq. (23) is controlled by the limiter b. The range of b, $1 \le b \le (3-\kappa)/(1-\kappa)$, is determined by condition of the TVD stability. Because b is larger, the region where the limiter function works becomes narrower.

IV. Numerical Results

The numerical example considered in this study is a laminar, turbulent entry flow through a three-dimensional square duct with a 90-deg bend. This bent duct flow is often used as a benchmark problem for three-dimensional flows,[15,16] and the curved square duct is a basic element for the actual flow devices. The computational geometry of the curved area is the same as the configuration studied experimentally by Taylor et al.[5] The inlet and outlet boundaries are located at $9H$ and $5H$ up and downstream from the bend. A no-slip boundary condition together with the Neumann condition for pressure was implemented on the solid wall boundary. Also, the uniform flow condition at the inlet boundary was prescribed. The control parameter b of 4 and κ of $\frac{1}{3}$ in Eq. (22) were used to guarantee as high an accuracy as possible in the application of the TVD scheme.

First, to investigate the numerical stability and convergence rate for the TVD application in the incompressible flow computation, Fig. 1 presents iteration histories of the norm of divergence. The norm of divergence, Eq. (1), is defined as

$$\text{norm of divergence} = \sqrt{\frac{1}{N}\sum_{ijk} D^2}$$

where N is the total number of grid points and i, j and k are the indices of each direction of ξ, η, and ζ, respectively. At the beginning of computation, the TVD scheme allowed the impulsive start with only the described boundary conditions. However, the other schemes required a starting value or careful attention to such factors as starting with a very small time increment and a prescription of velocity and pressure fields even if it is a laminar flow of $Re = 790$. Therefore, all computations to compare the convergence rates were performed with a starting value obtained from precomputation by the TVD scheme with 400 iterations.

The effect of applying the TVD scheme to the laminar flow with Reynolds number $Re = 790$ is remarkable in the iteration histories, where a body-fitted coordinate grid with $107 \times 41 \times 41$ points was used and the streamwise spacing at the bend area is 2.5 deg. In the case of the third-order upwind and QUICK scheme, the norms are still in the range of the order of 10^{-5} after 6000 iterations, and they are somewhat unstable. With the TVD scheme, however, a rapid convergence rate is obtained. In this laminar flow, the tendency of the stability and that of the convergence rate of the TVD scheme are similar to those of the MQUICK scheme, which is an improved QUICK scheme for the incompressible flow.

Figures 2 and 3 show some comparisons of streamwise velocity U and radial velocity W profiles along the spanwise direction

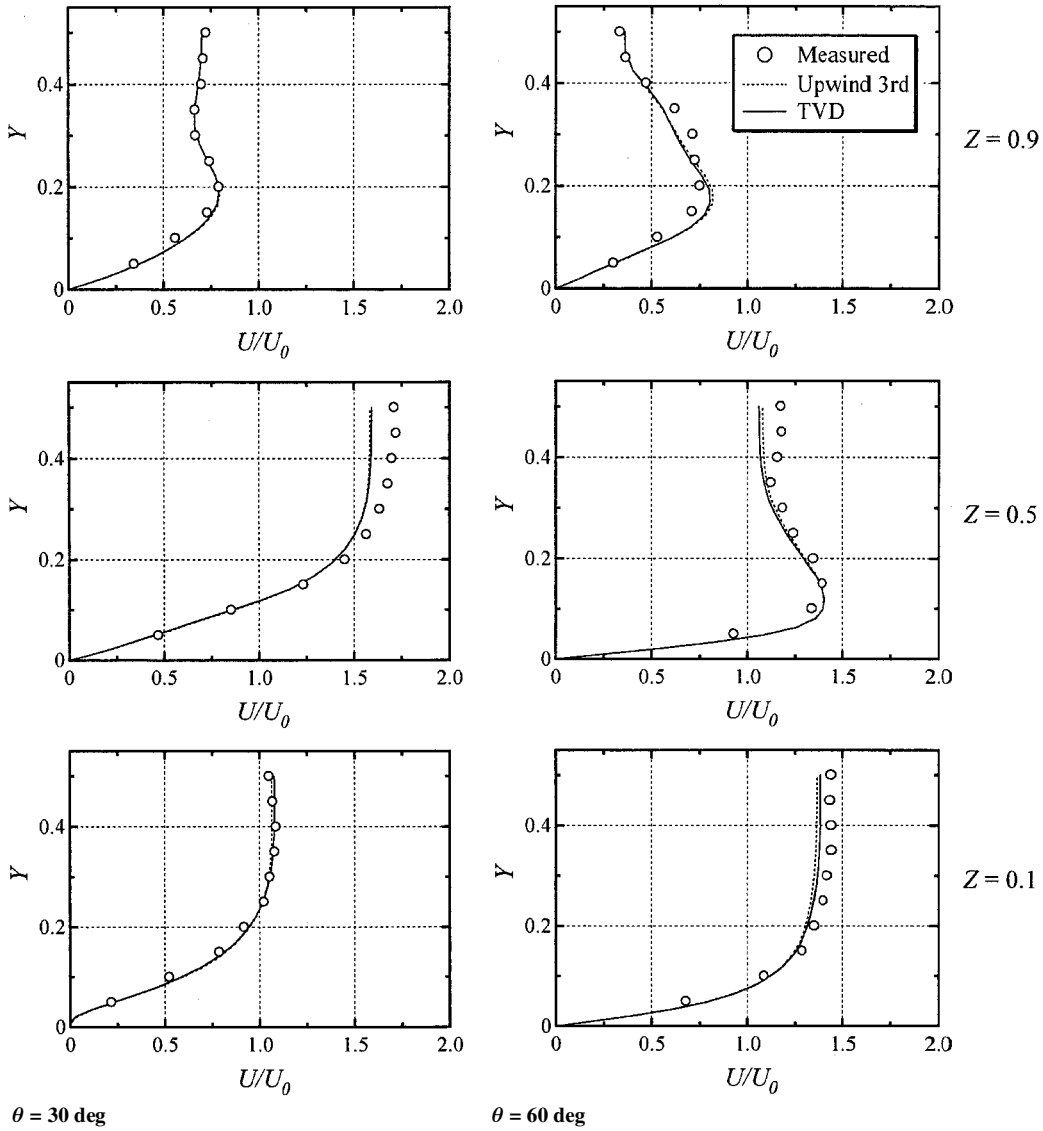

Fig. 2 Comparison of streamwise velocity profiles.

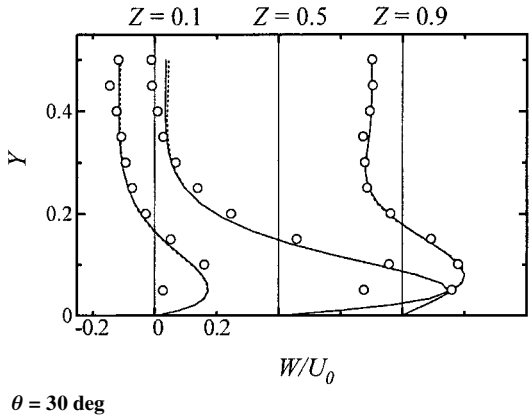

θ = 30 deg

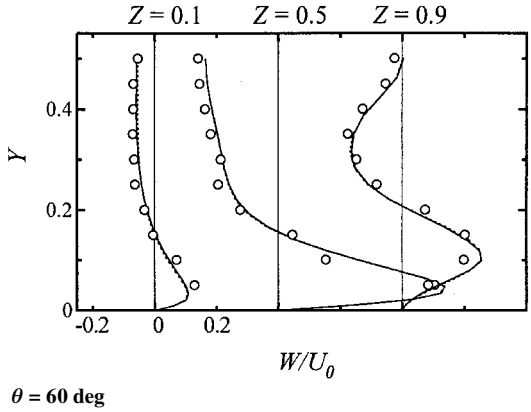

θ = 60 deg

Fig. 3 Comparison of radial velocity profiles: - - -, third-order upwind scheme; ——, TVD scheme; and○, measurements.

Y with experiments[5] at several streamwise locations. Here θ is a turning angle measured from the start of the bend. The agreement between predictions and measurements is quite good at most locations. The present computations well capture the peak value of each velocity component and all of the qualitative features of the flow. The discrepancy between the result obtained by the TVD scheme and that by the third-order upwind scheme is very small, so that from Figs. 1–3, it is shown that the numerical method using the TVD scheme is more efficient than the others.

Figure 4 shows computed streamwise velocity contours compared with contours derived from the measurements[5] at four streamwise locations. These results by the TVD scheme show good quantitative agreement with the measurement as a whole. This shows that the center of the high-velocity flow moves to the outer wall with the angle of θ and up to about $2H$ downstream of the bend, which is due to the secondary flow formed by the curvature. At 30 and 60 deg in the bend, the computed velocities gradually roll up the flow into a passage vortex. Then, at $X_H = 0.25H$ and $X_H = 2.5H$ downstream from the bend, they show the decay of the vortex. These redistributions of the streamwise velocity agree very well with measurements. Also, a recirculation zone exists at the corner of the outside wall at the 30-deg plane in Fig. 4.

Figure 5 shows the distribution of the order of accuracy of applying the TVD scheme to an incompressible laminar flow. This indicates that the accuracy is in the range over second order in all computational regions. Therefore, we know that there is no problem with regard to the sharp loss of accuracy, which will occur due to the working of the minmod function as we experienced in the compressible flow computation.

In a manner similar to the laminar flow calculation, turbulent flow with a Reynolds number of $Re = 4 \times 10^4$ was computed. A body-fitted coordinate grid with $135 \times 61 \times 61$ points was used, and the streamwise spacing at the bend area was 2 deg. In the present turbulent flow simulation, QUICK and even MQUICK upwind schemes

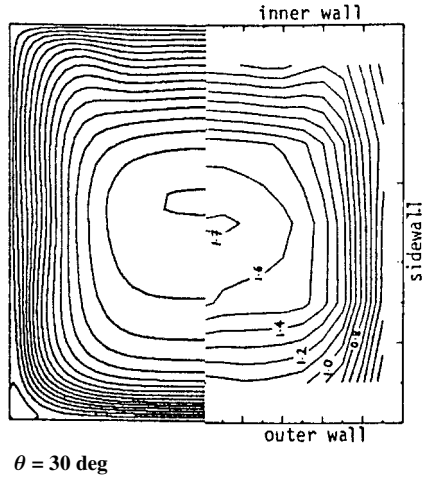

θ = 30 deg

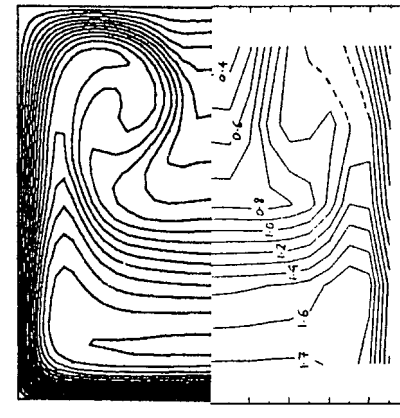

X_H = 0.25

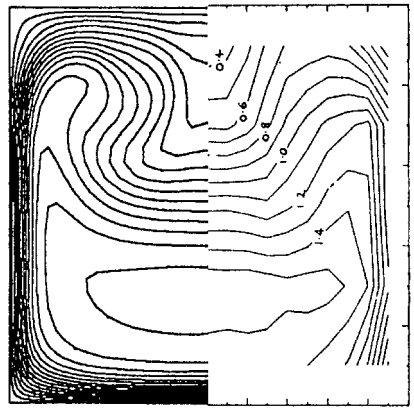

θ = 60 deg

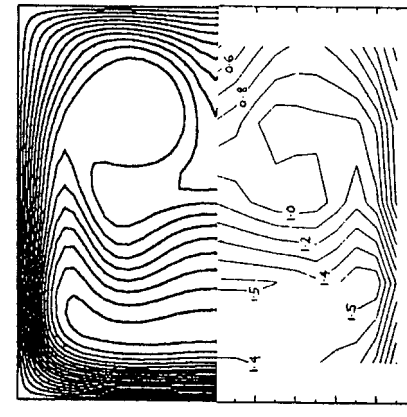

X_H = 2.5

Fig. 4 Comparison of streamwise velocity contours with experiments at several streamwise stations. In each panel, results from computations are shown on the left and from experiments on the right.

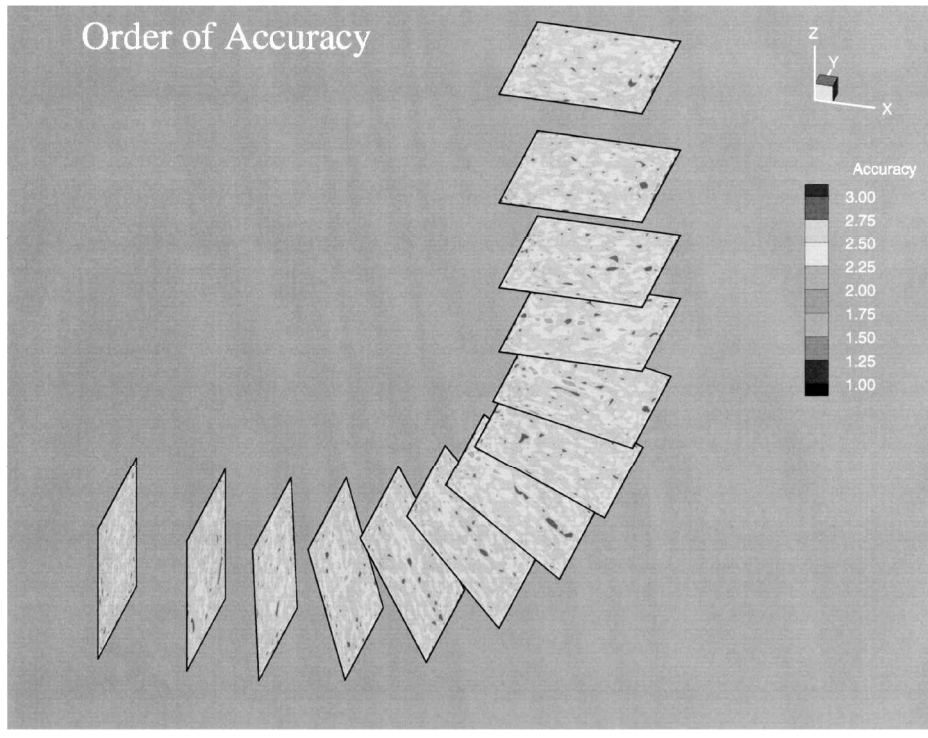

Fig. 5 Distribution of the order of accuracy for TVD scheme.

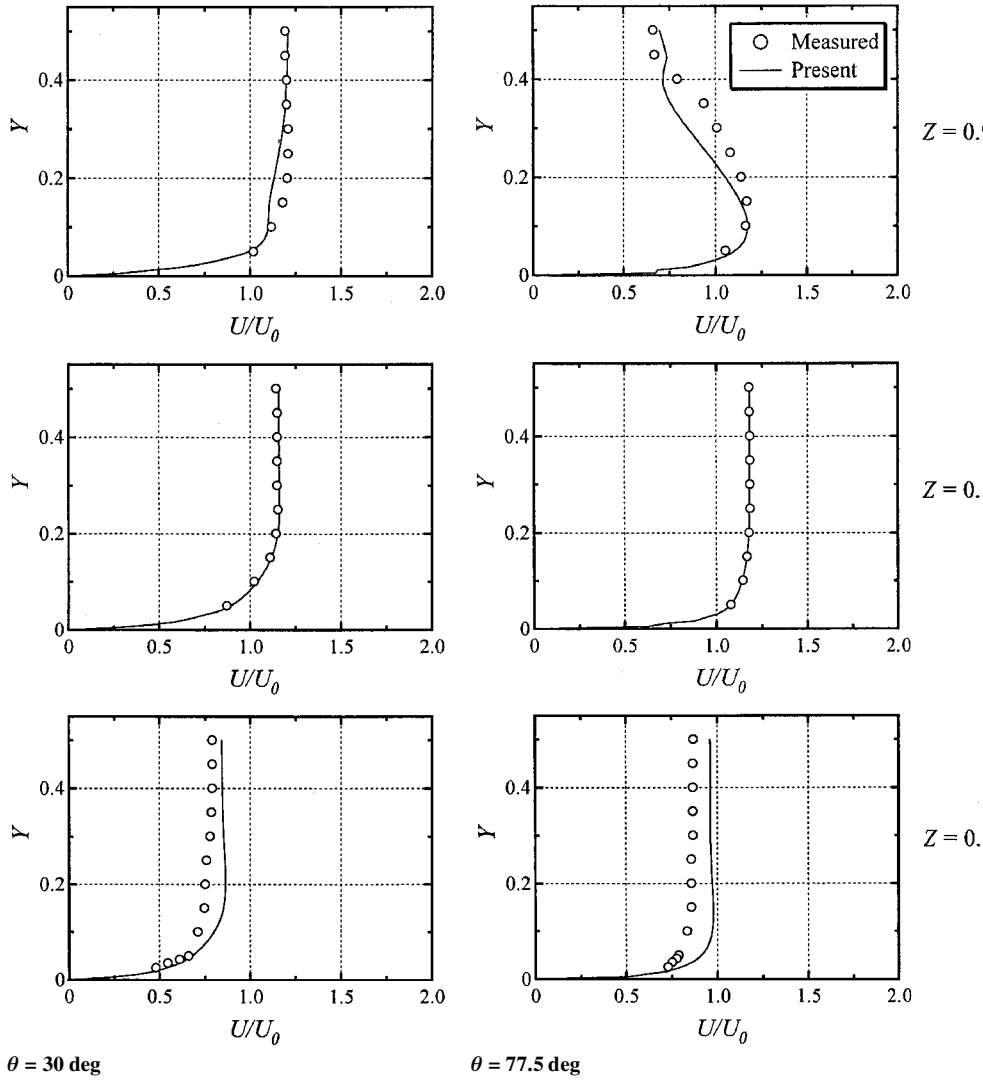

Fig. 6 Comparison of time-averaged streamwise velocity profiles (turbulent flow).

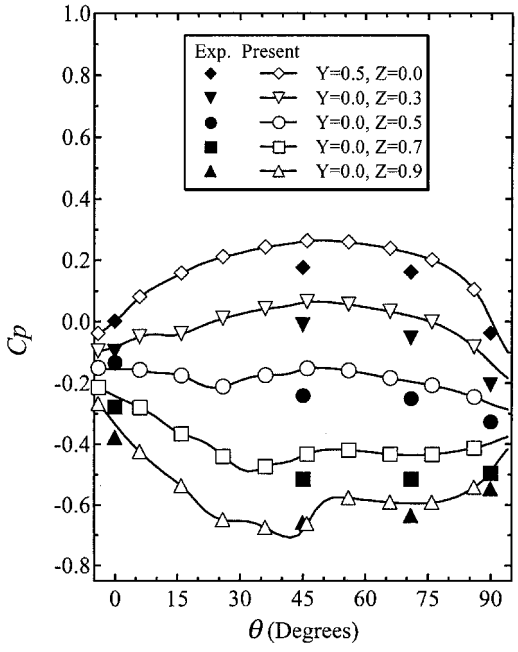

Fig. 7 Comparison of time-averaged wall pressure distributions (turbulent flow).

could not reduce the instability at relatively high Reynolds number and a strong curved flowfield, although they well simulated the earlier laminar flows. This is because, even though the incompressible flow is milder than the compressible flow, unsteady turbulent flow with high Reynolds number sometimes leads to the local extreme because of geometrical effects such as squared corners and strong curvature.

The steady flow computation was first carried out to obtain the starting value for unsteady computation. Then unsteady turbulent flow computation was performed with the Crank–Nicholson method and the LES method for the SGS turbulence. The Smagorinsky constant C_s of 0.1 is chosen in Eq. (5), and the grid scale Δ is modified to $\Delta = \min(\Delta_\xi, \Delta_\eta, \Delta_\zeta)$ because the diagonal volume length or the geometric mean length results in overestimation of the SGS viscosity for the present relatively coarse grid, which has the already mentioned grid points and a grid size of $0.005H$ as the smallest value in both the Y and the Z (radial) directions. Also, to take near-wall effects into account, the Van Drist wall-damping function $f_d[=1-\exp(-y^+/A^+)]$ was imposed on ν_s in Eq. (5) with an empirical coefficient A^+ of 26.

Figure 6 shows some comparisons of time-averaged streamwise velocity profiles along the Y with laser Doppler velocimetry (LDV) measurements[5] at several streamwise locations. As seen in Fig. 6, comparisons of computed streamwise velocities with measurements are quite good everywhere. In this turbulent flow, the strength of the redistribution of the streamwise flow is smaller than that of the laminar flow in Fig. 2 due to the difference in the thickness of the inlet boundary layers.

Figure 7 presents the wall pressure distribution along the streamwise θ direction. Predicted pressure coefficients $C_p = 2(p - p_{\text{ref}})/\rho U_0^2$ with p_{ref} of the pressure at 0 deg, $Z = 0$, and the midspan compare very well with measurements. An adverse pressure gradient develops on the outside wall (at $Z = 0.1$) up to $\theta \approx 50$ deg, and then the pressure gradient is reversed with θ due to the flow deceleration and acceleration as shown in Fig. 6. On the inside wall, the pressure gradient shows a converse trend as expected. Relatively high pressure is distributed near the outside wall and the pressure loss recovers downstream of the bend.

V. Conclusions

A stable finite difference method in which a TVD upwind scheme is applied was proposed to solve the incompressible Navier–Stokes equations. The numerical method is based on the efficient implicit SMAC scheme previously developed to solve these equations in general curvilinear coordinates. The validity and receptivity of the application was investigated through the examination of the accuracy, stability, and convergence rate.

For this investigation, a three-dimensional developing entry laminar and turbulent flow through a square duct with a 90-deg bend was calculated using the finite difference method and compared with numerical results obtained by QUICKs and the third-order upwind schemes and LDV measurements. Predictions by the TVD scheme showed good agreement with experiments, and accurate simulations of three-dimensional complex flow characteristics including the redistribution of the streamwise velocity and strong secondary motion in the bend were successfully shown.

In the comparison of stability and convergence rate with QUICKs and the third-order upwind scheme, the implicit method using the TVD scheme was found to be the most stable and to have the highest computational efficiency. It was confirmed that there is no sharp drop in accuracy because the working of the limiting procedure of the TVD scheme is much rarer than that of compressible flow simulation. However, this limiting procedure plays an important role to simulate practical incompressible flows with local extremes. In view of the results so far obtained, the TVD scheme can be used with confidence for incompressible flow computations.

References

[1]Leonard, B. P., "A Stable and Accurate Convective Modeling Procedure Based on Quadratic Upstream Interpolation," *Computer Methods in Applied Mechanics and Engineering*, Vol. 19, 1979, pp. 59–98.

[2]Shin, B. R., Ikohagi, T., and Daiguji, H., "A Modified QUICK Scheme with Good Stability and High Convergence Rate," *Computational Fluid Dynamics Journal*, Vol. 7, No. 3, 1998, pp. 283–299.

[3]Harten, A., "High Resolution Schemes for Hyperbolic Conservation Laws," *Journal Computational Physics*, Vol. 49, No. 3, 1983, pp. 357–393.

[4]Chakravarthy, S. R., and Osher, S., "A New Class of High Accuracy TVD Schemes for Hyperbolic Conservation Laws," AIAA Paper 85-0363, Jan. 1985.

[5]Taylor, A. M. K., Whitelaw, J. H., and Yianneskis, M., "Curved Ducts with Strong Secondary Motion: Velocity Measurements of Developing Laminar and Turbulent Flow," *Journal of Fluid Engineering*, Vol. 104, No. 9, 1982, pp. 350–359.

[6]Cabuk, H., Sung, C. H., and Modi, V., "Explicit Runge–Kutta Method for Three-Dimensional Internal Incompressible Flows," *AIAA Journal*, Vol. 30, No. 8, 1992, pp. 2024–2031.

[7]Ikohagi, T., and Shin, B. R., "Finite-Difference Schemes for Steady Incompressible Navier–Stokes Equations in General Curvilinear Coordinates," *Computers and Fluids Journal*, Vol. 19, No. 3/4, 1991, pp. 479–488.

[8]Shin, B. R., Ikohagi, T., and Daiguji, H., "An Unsteady Implicit SMAC Scheme for Two-Dimensional Incompressible Navier–Stokes Equations," *Japan Society of Mechanical Engineers International Journal*, Ser. B, Vol. 36, No. 4, 1993, pp. 598–606.

[9]Smagorinsky, J., "General Circulation Experiments with the Primitive Equations," *Monthly Weather Review*, Vol. 91, No. 3, 1963, pp. 99–164.

[10]Beam, R. M., and Warming, R. F., "Implicit Factored Scheme for the Compressible Navier–Stokes Equations," *AIAA Journal*, Vol. 16, No. 4, 1978, pp. 393–402.

[11]Shin, B. R., Ikohagi, T., and Daiguji, H., "An Implicit Finite Difference Scheme for the Incompressible Navier–Stokes Equations Using an Improved Factored Scheme," *Computational Fluid Dynamics Journal*, Vol. 4, No. 2, 1995, pp. 191–208.

[12]Hirt, C. W., Nichols, B. D., and Romero, N. C., "SOLA-A Numerical Solution Algorithm for Transient Fluid Flows," Los Alamos Scientific Lab., Rept. LA-5852, Los Alamos, NM, 1975.

[13]Patankar, S. V., and Spalding, D. B., "A Calculation Procedure for Heat, Mass and Momentum Transfer in Three-dimensional Parabolic Flows," *International Journal of Heat and Mass Transfer*, Vol. 15, No. 10, 1972, pp. 1787–1806.

[14]Chakravarthy, S. R., "Development of Upwind Schemes for the Euler Equations," NASA CR 4043, Jan. 1987.

[15]Govindan, T. R., Briley, W. R., and McDonald, H., "General Three-Dimensional Viscous Primary/Secondary Flow Analysis," *AIAA Journal*, Vol. 29, No. 3, 1991, pp. 361–370.

[16]Rosenfeld, M., Kwak, D., and Vinokur, M., "A Fractional Step Solution Method for the Unsteady Incompressible Navier–Stokes Equations in Generalized Coordinate Systems," *Journal of Computational Physics*, Vol. 94, No. 1, 1991, pp. 102–137.

R. M. C. So
Associate Editor